Scientific Research Publishing

Materials Sciences and Applications, 2024, 15, 481-503
https://www.scirp.org/journal/msa
ISSN Online: 2153-1188
ISSN Print: 2153-117X

New Flexible Electrospun PET/TiO_2 Composite Photoanode Layer for Dye-Sensitized Solar Cells, DSSCs, and Its Photovoltaic Performances

Hajer Gallah[1,2], Frej Mighri[1,2*], Abdellah Ajji[1,3], Jayita Bandyopadhyay[2,4], Nouceir Ahmed Ben Ghorbel[1,2], Judith Castillo-Rodriguez[5]

[1]Research Center for High Performance Polymer and Composite Systems (CREPEC), Department of Mechanical Engineering, McGill University, Montreal, Canada
[2]Department of Chemical Engineering, Laval University, Quebec, Canada
[3]Department of Chemical Engineering, Polytechnique Montreal, Montreal, Canada
[4]Center for Nanostructures and Advanced Materials, Council for Scientific and Industrial Research, Pretoria, South Africa
[5]Department of Chemistry and Biology, Toronto Metropolitan University, Toronto, Canada
Email: *frej.mighri@gch.ulaval.ca

How to cite this paper: Gallah, H., Mighri, F., Ajji, A., Bandyopadhyay, J., Ghorbel, N.A.B. and Castillo-Rodriguez, J. (2024) New Flexible Electrospun PET/TiO_2 Composite Photoanode Layer for Dye-Sensitized Solar Cells, DSSCs, and Its Photovoltaic Performances. *Materials Sciences and Applications*, **15**, 481-503.
https://doi.org/10.4236/msa.2024.1511033

Received: October 16, 2024
Accepted: November 15, 2024
Published: November 18, 2024

Abstract

Flexible polymer-based dye-sensitized solar cells (DSSCs) offer promising potential for lightweight, cost-effective and versatile photovoltaic applications. However, the critical challenge in their widespread applications is the weak thermal stability of most polymeric substrates, which can only withstand a maximum temperature processing of 150˚C. In this study, a facile and low-cost strategy is proposed to develop at low temperature DSSC flexible photoanode based on a polymeric matrix. Highly porous nanocomposites fibrous mats composed of polyethylene terephthalate (PET) and titanium dioxide (TiO_2) nanobars were prepared through an electrospinning process using different configurations (uniaxial electrospinning, coaxial electrospinning, and electrospray-assisted electrospinning). These techniques enabled precise control of the microstructure and the positioning of TiO_2 within the composite nanofibers. Therefore, the as-produced photoanodes were loaded with N719 dye and tested in DSSC prototype using iodide-triiodide electrolyte and platinum (Pt) coated counter electrode. The results show that incorporating TiO_2 on the fiber surface through the electrospray-assisted electrospinning enhanced the performance of the nanofiber composite, leading to improved dye loading capacity, electron transfer efficiency and photovoltaic performance.

Keywords

Electrospinning, Electrospraying, Coaxial Electrospinning, Nanocomposites, Nanofibers, Flexible DSSCs, Photoanode, TiO_2

1. Introduction

The growing need for sustainable energy solutions has driven the exploration of innovative technologies to harness renewable resources efficiently. Among these technologies, Dye-sensitized solar cells (DSSCs), classified as third generation of photovoltaic technology, emerge as promising solar cells due to their cost-effectiveness, stability, ease of fabrication and reasonable efficiency in diverse light conditions [1]. DSSCs are primarily composed of three components: photoanode, a liquid electrolyte and a catalytic counter electrode [2]. The photoanode layer typically consists of a 10 μm thick mesoporous TiO_2 film sensitized by dye and coated onto a transparent conductive substrate. It plays a central role in the cell's operation, serving two essential functions. First, it acts as a support structure for loading the dye. Second, it facilitates the transport of electrons from the dye to the external circuit [3]. Upon illumination of the photoanode by visible light, the dye molecules in the photoanode undergo photoexcitation, generating excited electrons. These photogenerated electrons are then injected into the TiO_2 conduction band and transported to the external circuit through the conductive substrate, producing an electric current [4]. Usually, the TiO_2 paste is applied to a brittle, rigid substrate coated on fluorine-doped tin oxide (FTO) glass, and then subjected to sintering at high temperatures ranging between 450˚C - 500˚C [5]. This thermal treatment is crucial for removing the organic binder, forming pores to facilitate efficient dye absorption, establishing electrical connectivity among TiO_2 nanoparticles, as securing a robust electrical contact between the TiO_2 layer and the substrate [6]. However, these conventional glass-based DSSCs present several limitations, including their lack of flexibility, fragility, significant weight, shape constraints, elevated cost, and incompatibility with industrial processing (roll-to-roll process) [7]. On the other hand, flexible plastic-based DSSCs offer notable benefits, such as being lightweight, flexible, portable, suitable for mass production, and cost-effective [8]. Moreover, the adoption of flexible plastic substrates broadens the potential applications of DSSCs, accommodating needs in sectors that require flexibility, such as building-integrated devices, wearable technology, and portable electronics [9]. Consequently, there has been push towards the development of flexible DSSCs using plastic substrates.

Developing flexible DSSCs poses significant challenges, primarily due to the limited thermal stability of plastic substrates, which can withstand temperatures up to only 150˚C [10]. Various studies have explored the creation of flexible porous TiO_2 photoanodes through low-temperature processes such as chemical sintering [11], electrodeposition [12], and mechanical compression [13]. Despite these efforts, these methods often encounter problems such as inadequate interparticle contact, compromised film integrity, and poor adhesion between the TiO_2 layer and the plastic substrate [14]. As a result, the TiO_2 films frequently develop cracks and are susceptible to detachment during bending, leading to device failure or rapid performance decline [12]. In practical applications, flexible DSSCs undergo repeated mechanical deformation, including bending, rolling,

and twisting, making the mechanical stability of the device just as critical as its photovoltaic performance [15].

To tackle the issue and boost the mechanical robustness of flexible DSSCs, considerable research has been dedicated to altering the photoanode structure via the incorporation of polymers [16]-[19]. Li *et al.* [16] investigated the incorporation of a small amount of polymethyl methacrylate (PMMA) (0 - 10 wt.%) into TiO_2 paste and produced photoanode layer through solution blending and subsequent sintering at 150˚C, followed by mechanical compression. While PMMA improved the photoanode's flexibility, it reduced pore size and compromised electrical contact between TiO_2 nanoparticles. In our previous work [19], we developed a porous polypropylene (PP)/TiO_2 flexible photoanode using melt extrusion followed by uniaxial stretching to create pores. The porosity increased with stretching ratio leading to higher dye adsorption. However, the overall porosity of the developed photoanodes remained low. This technique struggled to balance cell's efficiency and mechanical strength, as the added polymer increased electrical resistance within the photoanode and, in excess, blocked the adsorption and slowed electron transport, negatively affecting the overall performance of the cell [17].

The electrospun nanofibrous mats, with high porosity, large surface-to-volume ratio, and tunable fiber morphology, are promising candidates for flexible DSSCs photoanodes due to improved dye loading and electrolyte penetration [20]. Most research utilizing the electrospinning process to develop photoanodes has focused on ceramic nanofibers [21]. However, the subsequent high-temperature calcination required to remove organic components often results in mechanically fragile ceramic nanofibers that can break into small aggregates or become powdery under external forces, leading to detachment from the substrate [22]. Li *et al.* [17] showed that electrospraying binder-free TiO_2 nanoparticles onto electrospun polyvinylidene fluoride (PVDF) nanofibers significantly enhanced the stability and mechanical durability of the photoelectrode. This approach of adding electrospun polymer fibers reduced stress within the photoanode during bending, thereby minimizing the risk of delamination by slowing the initiation and propagation of cracks. The efficiency of the flexible photoanode was comparable to conventional DSSCs, demonstrating that a TiO_2 structure within a porous polymeric matrix can enhance both efficiency and durability in flexible DSSCs

This study aims to create novel functional PET/TiO_2 composite nanofibrous mats using a low-temperature electrospinning technique and evaluate their effectiveness as flexible photoanodes in DSSC. To construct the flexible, composite fiber-based photoanodes, various methods including uniaxial electrospinning, coaxial electrospinning, and electrospray-assisted electrospinning were employed. These techniques allow for precise control over the nanofibers' microstructure and the selective distribution of TiO_2 particles within them. Specifically, by confining TiO_2 nanoparticles to the nanofibers' outer layer (the shell) using coaxial electrospinning, or by affixing them to the fibers' surface via electrospray-assisted

electrospinning, the study seeks to enhance the interaction between TiO_2 and the dye molecules. Such optimization aims to improve light absorption and electron transport efficiency within the DSSC's photoanode, contributing to the development of more efficient solar cells.

Polyethylene terephthalate (PET) was chosen as the fiber's matrix owing to its notable structural and mechanical qualities. To achieve superior dispersion within the polymer solution, surfactant-capped TiO_2 nanobars (referred to as $TiO_{2,NB}$) were utilized, replacing the traditional commercial Degussa P25 TiO_2. The adoption of one-dimensional (1D) TiO_2 is anticipated to establish a direct pathway for electron transport, enhancing rapid charge collection and minimizing recombination events [23]. To the best of our knowledge, this is the first time such a structure to be used as flexible photoanodes in DSSC applications.

2. Materials and Methods

2.1. Materials

The following chemicals were used in this work as received without further purification. Titanium (IV) butoxide (TB, 97%), oleic acid (OA, 90%), oleylamine (OM, 70%), absolute ethanol and toluene (analytical grade) were purchased from Sigma Aldrich, Canada. Polyethylene terephthalate (PET) pellets (Laser + C9921) were purchased from DAK Americas, USA. Electrospinning/Electrospray solvents, trifluoroacetic acid (TFA) and dichloromethane (DCM), which were all analytical grade, were respectively supplied from Alfa AESAR, and Acros Organic, Canada. N719 industry standard dye Di-tetrabutylammonium cis-bis(isothiocyanato)bis(2,2'-bipyridyl-4,4'-dicarboxylato)ruthenium(II)) was purchased from Fisher Scientific, Canada. Indium tin oxide/polyethylene terephthalate substrate (ITO/PET, thickness of 175 μm, 20 - 30 Ω sq^{-1}) was provided by MSE Suppliers, USA. Platinum-coated fluorine doped tin oxide glass counter electrode (Pt-FTO/glass) and Iodolyte AN-50 high performance electrolyte (Iodide based) were purchased from Solaronix, Switzerland.

2.2. Synthesis of $TiO_{2,NB}$

The synthesis of $TiO_{2,NB}$ shown in **Figure 1** was conducted via a solvothermal method, in the presence of OA and OM as capping agents, as previously described in our work [24]. Initially, 1 mmol of TB was mixed with 6 mmol of OA and 4 mmol of OM. This mixture was then stirred for 15 min, after which 1 ml of absolute ethanol was added, followed by another 15 min of stirring. The mixture was then placed inside a Teflon cup, which was subsequently transferred to a Teflon-lined stainless-steel autoclave filled with 4 ml of ethanol 95%. The autoclave was heated inside an oven at 150˚C for 18 h. Upon cooling to room temperature, the resulting TiO_2 nanoparticles, appearing as white solid precipitate powder), were collected by vacuum filtration and washed at least four times with ethanol and toluene. The final product was left to dry at room temperature for 24 h.

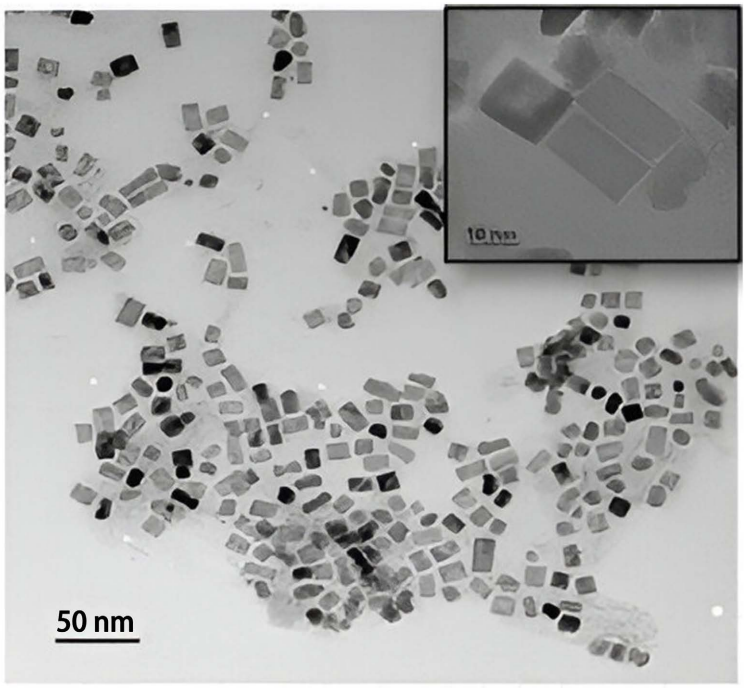

Figure 1. TEM image of surfactant-capped $TiO_{2,NB}$ used in this work [24].

2.3. Development at Low Temperature of Composite Fiber-Based DSSC Photoanode Layer

Well-dispersed electrospinning solutions of PET and PET/$TiO_{2,NB}$ were prepared by initially dissolving 1.5 gr of PET in 10 ml mixture of TFA/DCM (70/30 v/v) mixture, stirring for 18 hours to ensure the PET was completely dissolved. For PET-TiO_2 solutions, $TiO_{2,NB}$ were incorporated into the polymer solution at a concentration of 15 wt.% relative to PET. The resulting mixture was then stirred for an additional 18 hours, followed by 2 hours of sonication at room temperature to ensure the TiO_2 nanoparticles were homogeneously dispersed. Immediately before the electrospinning process, each solution underwent an additional 5 minutes of sonication to prevent nanoparticles agglomeration. For the electrospray solution, 7 wt.% of $TiO_{2,NB}$ was dispersed in the solvent by stirring for 3 hours and then sonicated for 15 minutes to achieve a well-dispersed mixture.

Flexible composite fiber-based photoanodes were developed using three distinct methods: uniaxial electrospinning (UE), coaxial electrospinning (CE), and a combined electrospinning/electrospray process (E-ES). The schematic diagrams of these fabrication techniques are depicted in **Figure 2**. To create the electrospun fibrous mats, a home-made laboratory-scale electrospinning setup was used. This setup consisted of two programmable syringe pumps (Pump 11 Elite by Harvard Instrument, USA, and NE-300 by Era Pump Systems Inc, USA), a high-voltage power supply (Chargemaster CM60-P by Simco, USA), and a grounded collector plate covered with aluminum foil. The aluminum foil was affixed to a 2 cm × 2 cm section of a transparent, conducting ITO-coated PET film, facilitating the direct deposition of the composite fibers onto the substrate.

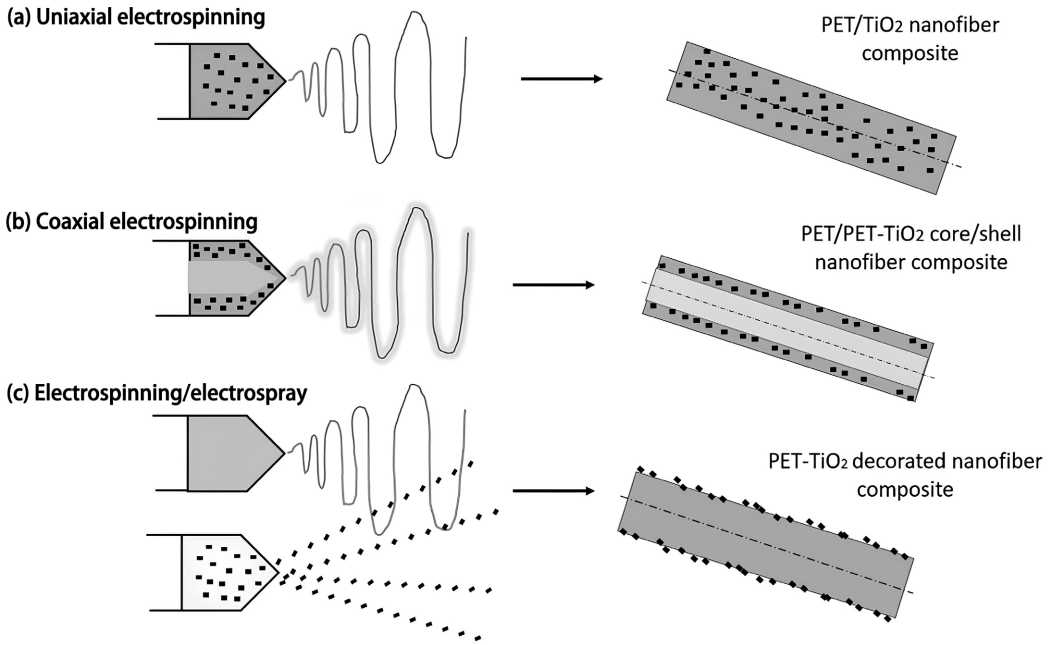

Figure 2. Schematic diagrams for the development of flexible composite-based photoanode: (a) Uniaxial electrospinning; (b) Coaxial electrospinning; (c) Electrospinning/electrospraying.

In the Uniaxial Electrospinning process, PET/$TiO_{2,NB}$ nanofibrous mats were fabricated by electrospinning a singular solution comprising PET and $TiO_{2,NB}$ nanoparticles. Conversely, the Coaxial Electrospinning process utilized two distinct solutions: one of PET for the core and another of PET/$TiO_{2,NB}$ for the shell. Detailed methodologies of the UE and CE processes are extensively documented in our work [23] [24]. In the Electrospinning-Electrospraying process, a PET solution was electrospun to form a PET nanofiber matrix, while concurrently, a $TiO_{2,NB}$ solution was electrosprayed onto the surface of the resulting mats.

The operational parameters for each method are concisely outlined in **Table 1**.

Table 1. Operating parameters for each process used in this study.

Process	Uniaxial electrospinning (UE)	Coelectrospinning (CE)	Electrospining-Electrospraying (E-ES)
Flow rate (ml/h)	1.0	Shell: 0.6 Core: 0.7	E: 1.0 ES: 0.5
Voltage (kV)	22.0	23.4	E: 23.4 ES: 18.0
Tip-to-collector distance (cm)	15.0	14.0	E: 14.0 ES: 10.0

2.4. DSSC Device Assembly

The production process of the DSSC device comprises multiple phases. Initially, the prepared photoanodes are submerged in a 0.3 mM solution of N719 dye dissolved in ethanol for 48 hours at ambient temperature. After this period, the

photoanodes are meticulously extracted from the dye solution and then washed with ethanol to eliminate any remaining dye that was not absorbed. Following this cleaning step, they are allowed to air dry in preparation for the assembly phase. The counter electrodes, which are Pt-coated FTO glass, were pre-treated with platinum and had pre-made holes for this experiment. Before incorporation into the cell, the components were washed with ethanol and subsequently subjected to heat treatment in a furnace at 450˚C for 20 minutes. This step is crucial for reactivating the catalytic Pt layer, thereby maximizing its performance. The assembly of the DSSC followed, arranged in a sandwich structure with the conductive sides of the electrodes facing inward towards each other. To prevent electrolyte evaporation and leakage, a 25 μm hot-melt Surlyn gasket served as the sealing agent. Heat and pressure were uniformly applied until the gasket achieved full adhesion to both electrodes.

Finally, the cell was filled with iodide-triiodide electrolyte through the pre-prepared hole in the counter electrode, using a vacuum-fill syringe. To finalize the assembly and ensure it was sealed, any excess electrolyte on the cell was carefully removed, and the holes were then covered with thin glass caps. These were sealed in place using a Surlyn sheet, which was bonded to the surface through resistive heating.

2.5. Dye Adsorption Characterization

Effective dye incorporation between the photoanode and the dye is crucial for the optimal performance of the DSSC. To measure dye loading, the dye is desorbed from the surface of the electrospun fibers by immersing them in a 0.1 M NaOH solution for 90 seconds. Initially, the nanofibrous mats are soaked in a 0.03 mM N719 dye solution in absolute ethanol for 48 hours, followed by rinsing with absolute ethanol to eliminate any unbound dye, and then air-dried at ambient temperature. The dye desorbed into the NaOH solution is then quantitatively analyzed through its optical absorption spectra using a UV-visible spectrophotometer (Carry 7000 model, Agilent, USA).

To provide a quantitative comparison of dye loading of the mat samples developed in this study, dye loading was estimated by the following equation [25]:

$$\text{Dye loading} = \frac{C \times V}{S} \tag{1}$$

where C (mol/L) is the concentration of adsorbed dye, V (L) the volume of the desorbed solution and S (cm^2) the active area of the nanofibrous mats (S = 0.25 cm^2 in this study). The concentration C of adsorbed dye was calculated by using the Lambert-Beer equation [26]:

$$C = \frac{A}{\varepsilon \times l} \tag{2}$$

where A is the UV-Vis absorbance peak intensity at 505 nm, $\varepsilon = 14.1 \times 10^3$ M^{-1} cm^{-1} is the molar extinction coefficient of N719 dye and l = 1 cm is the length of the optical path.

2.6. DSSC Photovoltaic Performance Characterization

The current-voltage (*J-V*) measurements were performed using a Keithley model 2400 digital source meter, interfaced with SciRunIV software for data acquisition. To simulate sunlight irradiation, a ScienceTech Xe solar cell simulator, with an AM1.5 G spectrum, was used. The light intensity calibration was achieved using a crystalline silicone (c-Si) as the reference cell. For photovoltaic performance evaluation, the DSSC devices were shielded with a black mask defining an active area of 0.25 cm^2. The fill factor (*FF*) and power conversion efficiency (PCE) were derived from the *J-V* curve using the following equations:

$$FF = \frac{I_{\max} \cdot V_{\max}}{J_{SC} \cdot V_{OC}} = \frac{P_{\max}}{J_{SC} \cdot V_{OC}} \tag{3}$$

$$\eta(\%) = \frac{P_{\max}}{P_{\text{in}}} \cdot 100 \tag{4}$$

where $I_{\max}$ is the maximum current density, $V_{\max}$ the maximum voltage generated at the maximum power point, $P_{\max}$. J_{SC} is the short circuit current density, V_{OC} is the open circuit voltage obtained by the DSSC under sunlight irradiation. P_{in} is the power of the sunlight illumination.

2.7. Electrochemical Impedance Spectroscopy (EIS) Characterization

In order to investigate the characteristics of the photoanode/dye/electrolyte interface and electron transport properties, an EIS analysis was carried out. This was performed using a Palmsens4 potentiostat (Bioanalytical Systems Inc., USA). The EIS experiments were conducted under a light irradiation intensity of 100 mW/cm^2, using a 150 W xenon arc lamp (ABET Technologies, Light Source LS 150). The frequency range for the measurements was established from 0.1 Hz to 100 kHz, with a 10 mV amplitude. The data gathered from the EIS study were then analyzed using ZView software for detailed insights into the electrochemical properties.

3. Results and Discussion

3.1. Morphology Characterization of the Developed Nanofibrous Photoanode Mats

In this study, various flexible nanofibrous photoanodes were developed by integrating $TiO_{2,NB}$ into the PET fiber framework using the three methods (UE, CE and E-ES) described above in Section 2.3. The surface morphology of the newly prepared photoanodes was assessed through Scanning Electron Microscopy (SEM) analysis and the corresponding images are shown in **Figure 3**. It was revealed by SEM images that the nanofibrous photoanode mats developed via UE and CE methods exhibited similar morphologies. Both types of photoanodes demonstrate a homogeneous porous structure characterized by bead-free and randomly oriented nanofibers. The distribution of TiO_2 nanoparticles within the

electrospun fibers prepared through both uniaxial and coaxial electrospinning methods has been elaborated on in our prior studies [23] [24]. In the uniaxial electrospinning (UE), TiO_2 nanoparticles predominantly scatter randomly within the PET fibers, with a considerable amount being enveloped by the PET polymer. Conversely, the coaxial electrospinning (CE) facilitates a more surface-oriented embedding of TiO_2 nanoparticles on the nanofibers, leading to the formation of a distinct core-shell structure, rather than being dispersed throughout the fiber. This is depicted in the inset of image (b) in **Figure 3**, showcasing the unique arrangement. On the other hand, the electrospinning-electrospraying (E-ES) method yields a noticeably different morphology. The electrosprayed TiO_2 nanoparticles are clearly present on the surface of the PET fibers, as evidenced by the SEM images (c) and (d). To further verify the surface deposition of TiO_2 on the fibers, energy dispersive X-ray (EDX) analysis was conducted, the results of which are presented in image (e) of **Figure 3**. EDX spectra confirmed the presence Ti element. For samples developed by E-ES, TiO_2 nanoparticles were deposited on the fiber surfaces as small spherical aggregates, thereby increasing the surface roughness. Additionally, the porous network revealed micropores filled with TiO_2 nanoparticles interspersed among the fibers. The deposition of TiO_2 within the electrospun fibers is a complex process that can be fine-tuned by adjusting various electrospray parameters such as TiO_2 concentration, spray distance, applied voltage, flow rate, and solvent composition. These parameters can impact the distribution of TiO_2 inside the mats on the fiber's surface and within the pores. In this study, the use of highly volatile chloroform solvent leads to rapid evaporation, causing TiO_2 to aggregate on the surface rather than entering the pores. Conversely, a lower TiO_2 concentration allows for more uniform infiltration into the micropores [17] [27] [28].

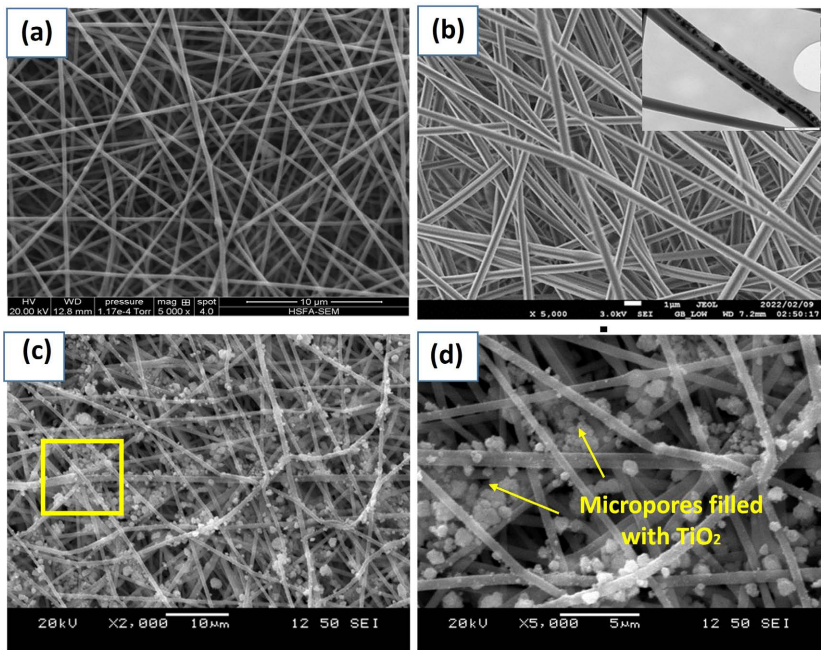

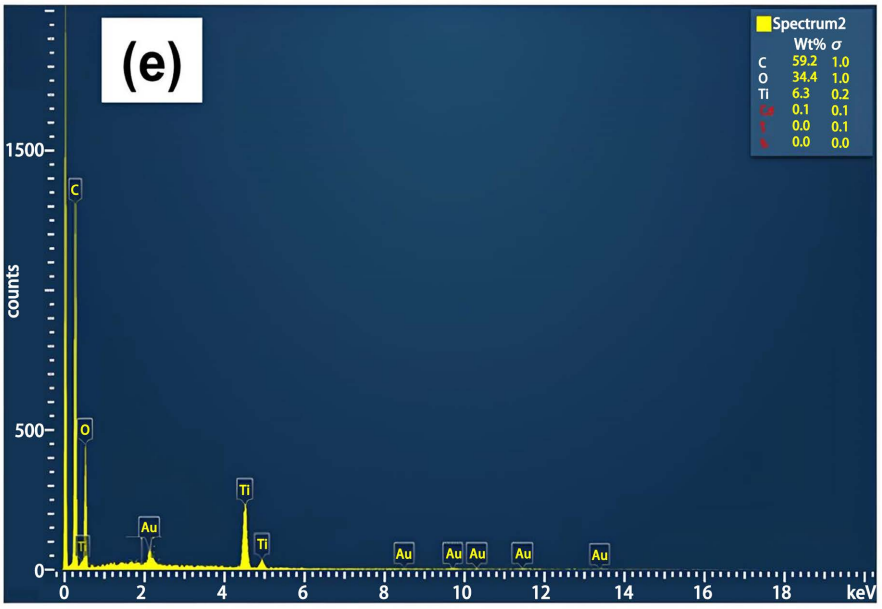

Figure 3. SEM images of flexible nanofibrous photoanode mats: (a) PET/TiO_2 nanofiber (UE); (b) PET/PET-TiO_2 core/shell nanofiber (CE); (c - d) PET-TiO_2 decorated nanofibers (E-ES); (e) Elemental composition of PET-TiO_2 decorated nanofibers (E-ES).

3.2. Dye Adsorption on the Surface of Nanofibrous Photoanode Mats

Dye adsorption entails the attachment of light-absorbing dye molecules to the photoanode's surface, a key process that significantly affects the DSSC's efficiency in transforming sunlight into electrical energy. To assess the dye adsorption capacity of the flexible nanofibrous photoanodes fabricated via the three methods (UE, CE, and E-ES), the photoanode mats were submerged in an N719 dye solution for 48 hours. Subsequently, the dye anchored to the surface of the electrospun fibers was desorbed using a NaOH basic solution. The absorption curves in the UV-visible spectrum for the desorbed N719 dye were meticulously analyzed and juxtaposed. **Figure 4(a)** and **Figure 4(b)** highlights the significant variations in dye adsorption capabilities across the developed nanofibrous mats. Notably, the PET-TiO_2 mats, synthesized via the electrospinning-electrospraying (E-ES) method, demonstrated a dramatic enhancement in N719 dye adsorption efficiency, recording increases of 110% and 337% when compared to coaxial electrospun (CE) PET/PET-TiO_2 core/shell mats, and uniaxial electrospun (UE) PET/TiO_2 mats, respectively. Despite the reduced porosity observed in the E-ES process compared to UE and CE processes, owing to the occlusion of micropores by TiO_2 agglomerates (as illustrated in **Figure 2**), the microstructural outcome presents a notable benefit. The E-ES process leads to a greater exposure of TiO_2 nanoparticles on the fiber surface along with enhanced surface roughness. This modification significantly boosts the adsorption capacity for N719 dye molecules, as evidenced by Ahmad *et al.* [29]. During the dye loading phase, a portion of the dye molecules becomes chemically bonded to the surface of the TiO_2 nanoparticles, whereas

others migrate into the porous framework of the nanofibrous mats [30]. For the mats developed by UE method, the random arrangement of TiO_2 inside the fibers, potentially covered by the PET polymer, hinders the entry and adsorption of dye molecules, leading to a decrease in dye loading efficiency. These findings align closely with the outcomes of morphological examinations presented above in Section 3.1.

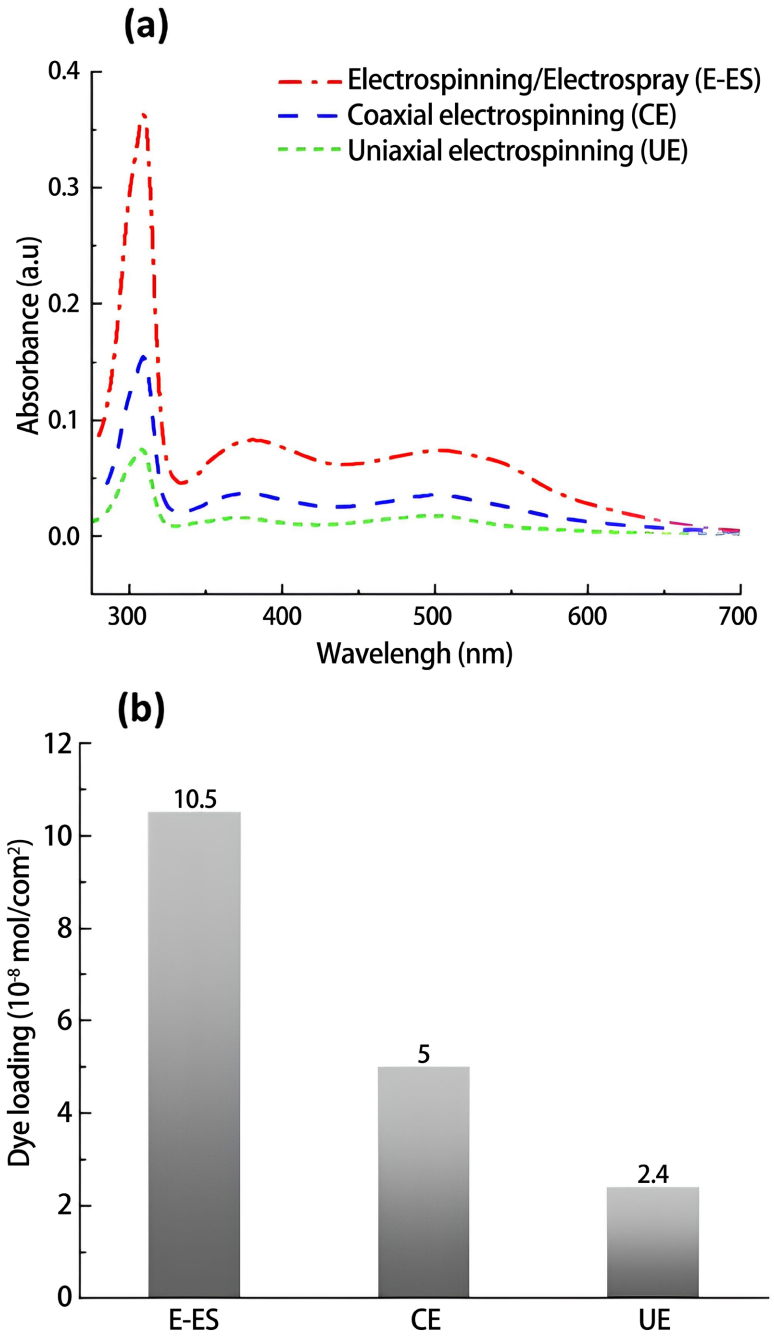

Figure 4. (a) UV-visible adsorption curves of the desorbed dye from the nanofibrous mats produced through E-ES, CE and UE techniques; (b) The corresponding amount of dye loading.

3.3. Current-Voltage (*J-V*) Characterization

The evaluation of the performance of the developed flexible nanofibrous photoanodes in a DSSC prototype was carried out by recording *J-V* curves under simulated solar irradiation, with the results presented in Figure 5. The DSSC performance parameters, including open-circuit voltage (V_{oc}), short-circuit current density (J_{sc}), fill factor (*FF*), and power conversion efficiency (η), derived from these plots, are compiled in Table 2. It is evident that the electrospinning-electrospraying method, which involves the decoration of PET nanofibers with TiO_2 nanoparticles, achieves the highest power conversion efficiency η at 0.03%. This is followed by coaxial electrospinning (CE) with an efficiency of 0.01%, while uniaxial electrospinning (UE) shows considerably poorer performance, resulting in significantly lower efficiency. The increased efficiency primarily stemmed from a notably higher J_{sc}. Table 2 demonstrates that the PET/TiO_2-decorated nanofiber-based photoanode, produced via the E-ES method, exhibited a current density of 0.12 mA/cm^2. This signifies a substantial 200% enhancement relative to the PET/PET-TiO_2 core-shell nanofiber-based photoanode, which had a current density of 0.04 mA/cm^2. Furthermore, a significant difference in J_{sc} was noted for the photoanode obtained with the UE method generating a current density two orders of magnitude lower than that of the CE method, despite both processes utilizing the same concentration of TiO_2 nanoparticles.

The decrease in J_{sc} suggests that fewer TiO_2 nanoparticles participated in the electron injection process, leading to a decreased light harvesting efficiency in DSSCs [31]. This finding underscores the vital importance of the strategic placement of TiO_2 nanoparticles on the nanofiber's surface to boost photovoltaic performance. Enhancements in J_{sc} are primarily driven by two factors: an increase in dye adsorption and a reduction in charge recombination [32]. For samples developed by the uniaxial electrospinning (UE) method, the TiO_2 nanoparticles were dispersed randomly within the fiber and encapsulated by the PET polymer, which obstructed the adsorption of dye molecules and hindered their access. PET's insulating nature impedes the flow of electrical charges, diminishing its photovoltaic efficiency. Conversely, the coelectrospinning (CE) method enables the positioning of TiO_2 nanoparticles on the outer layer (fiber shell), increasing the PET-free surface area available to these nanoparticles. This enhancement allows for better access to dye molecules, thereby improving dye adsorption and elevating the short-circuit current density (J_{sc}). In the electrospinning-electrospraying (E-ES) method, a marked improvement in dye loading was observed, attributed to the greater presence of TiO_2 nanoparticles on the PET nanofiber surface. This increase in dye/TiO_2 interaction boosts the electron injection rate and their transfer to the external circuit, leading to a higher J_{sc} [33]. Moreover, the open-circuit voltage (V_{oc}) and fill factor (*FF*) displayed no significant variation between the samples developed by both CE and E-ES methods. However, both parameters experienced notable declines for photoelectrodes developed using the UE method. The V_{oc}, which is largely determined by the energy gap between the Fermi level of TiO_2 and

the electrolyte's redox potential, decrease when increased charge recombination occurs [34], as observed in this study. This implies that with TiO_2 nanoparticles positioned inside the fiber developed by the UE method, more electrons are diverted through non-productive paths rather than contributing to current generation. Also, the *FF*, indicative of cell performance quality, saw a significant drop, pointing to reduced conductivity and a rise in the device's series resistance [35].

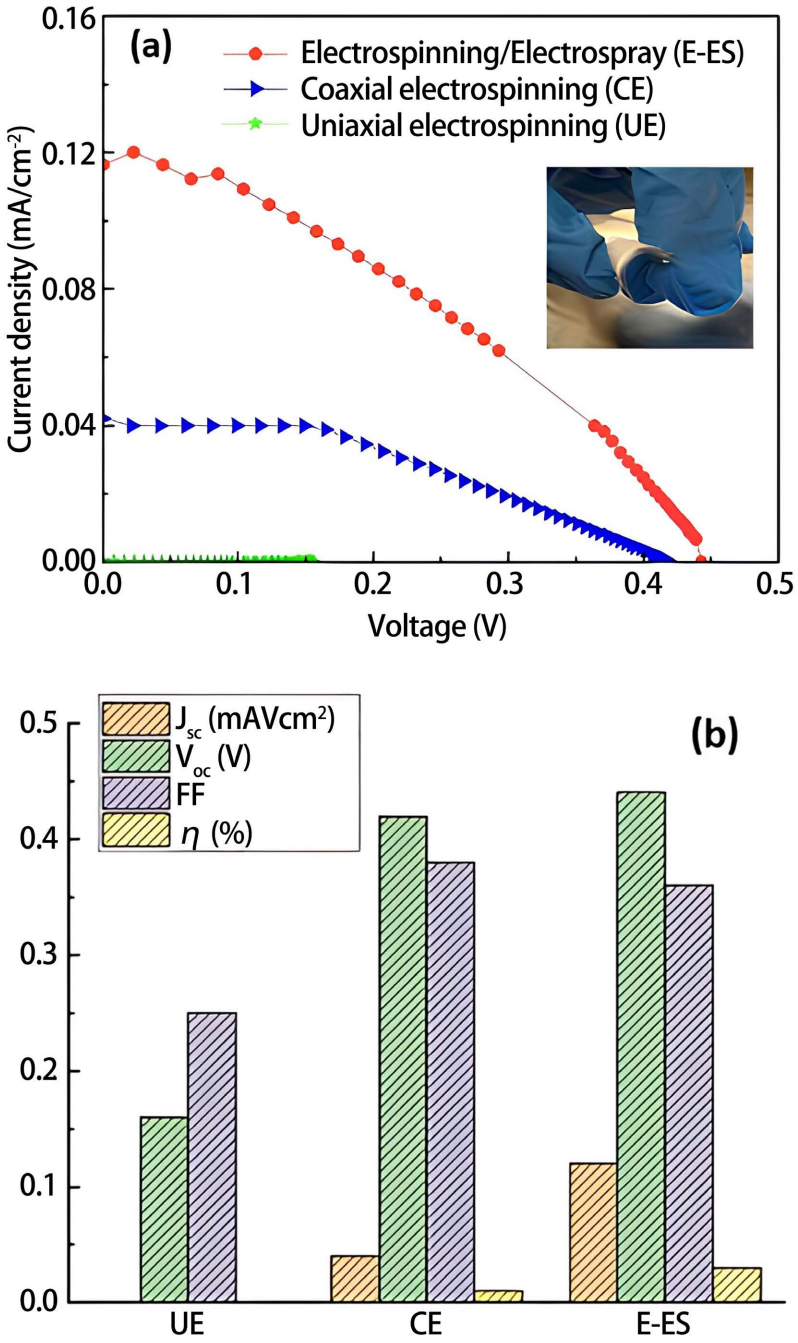

Figure 5. (a) J-V curves of DSSCs prepared using flexible nanofibrous photoanode mats produced through E-ES, CE and UE methods; (b) Their corresponding photovoltaic parameters.

Table 2. Photovoltaic parameters of DSSC prototypes using flexible nanofibrous photoanode mats developed using different electrospinning methods.

Electrospinning method used	J_{sc} (mA/cm²)	V_{oc} (V)	*FF*	η (%)	R_s (Ω)	R_{ct} (Ω)
UE	0.0003	0.16	0.25	1.8×10^{-3}	-	-
CE	0.04	0.42	0.38	0.01	431	2741
E-ES	0.12	0.44	0.36	0.03	762	2214

Most research on flexible electrodes has primarily focused on depositing a pure TiO_2 layer onto flexible substrates using low-temperature techniques or incorporating minor polymer quantities into the electrode structure, which has resulted in higher efficiencies compared to our study [36] [37]. To the best of our knowledge, the use of polymeric photoanodes is infrequently reported, and their efficiencies are not well documented. For instance, the work of Sa'adah *et al.* [18] evaluated a Polyacrylonitrile (PAN)/TiO_2 porous structure-based photoanode created through an electrospinning process and annealed on FTO/glass at 200˚C. The corresponding cells produced nanoampere-level photocurrents, with the most efficient cell reaching 365 nA, cell efficiency range was not discussed in their study. A significant limitation of this study was its restricted flexibility; the high processing temperature made it unsuitable for use on ITO/PET substrates. In previous research by our group [19] [38], a polypropylene (PP)/TiO_2 porous and flexible thin film was prepared using melt extrusion followed by uniaxial stretching. This material served as a flexible photoelectrode for DSSCs. The photoanodes exhibited a relatively low porosity of approximately 50%, which limited the dye-loading capacity. The highest-performing cell from this earlier study achieved a short-circuit current density (J_{sc}) of only 0.7 μA/cm², which is significantly lower than the results of the current study by at least two orders of magnitude. Additionally, the open-circuit voltage (V_{oc}) did not exceed 0.12 V. In our current work, the V_{oc} has been enhanced by approximately four fold. Another study [39] explored one-dimensional TiO_2 nanorods-based photoanodes on flexible Ti foil, achieving a J_{sc} of 0.14 mA/cm², a V_{oc} of 0.45 V, and an efficiency (η) of 0.03%, closely mirroring our results. However, the significantly higher cost of Ti foil compared to ITO/PET raises concerns regarding its commercial viability.

Nonetheless, the overall efficiency value of our work remains significantly lower than the values reported value by Li *et al.* [17]. This group achieved a 4% efficiency using a PVDF/TiO_2 fiber-reinforced composite-based photoanode on an ITO/PET substrate, which was compressed at 80 MPa. The compression post-treatment significantly altered the photoanode structure, as it creates a unique configuration where TiO_2 was embedded in and surrounded the PVDF fiber. This formed a highly interconnected TiO_2 network that adhered tightly to the PVDF fiber, thereby enhancing the short-circuit density (J_{sc}). In contrast, the low performance of our DSSC prototype can be attributed to the weak interparticle connections of TiO_2 nanoparticles and poor adhesion between the photoanode layer with the

substrate. This was due to the elemination of the sintering step and compression post-treatement, which hindered effective electron transfer within the cell. Another contributing factor to the lower performance could be the higher proportion of PET polymer in the composite, which may cause the TiO_2 nanoparticles to be coated by the PET polymer, reducing the electrical contact and thus impeding charge transfer through PET/TiO_2 nanocomposites. Additionally, our research deviates from standard practices by not using the commercial TiO_2 P25. Instead, we used surfactant-capped TiO_2 to enhance its dispersion within the PET solution. While surfactants improve dispersion, they may also obstruct electron transfer, potentially decreasing the efficiency of the DSSCs. Table 3 summarizes the DSSC performances of previously reported flexible photoanodes. While surfactants enhance the dispersion of TiO_2, they can also impede electron transfer, potentially reducing the efficiency of DSSCs. Capping ligands, such as oleylamine and oleic acid, has been shown to alter the energy levels of TiO_2, affecting the band alignment crucial for efficient electron transfer, as discussed in our previous work [40]. These modifications can hinder the effective movement of electrons to the conductive substrate or electrolyte, negatively impacting DSSC performance.

Table 3. Comparison of photovoltaic parameters from literature with this work.

Photoanode layer	Substrate	Deposition method/ post-treatment	Sintering temperature (˚C)	V_{oc} (V)	J_{sc} (mA/cm²)	FF	η (%)	Ref.
TiO_2/PET	ITO/PET	Electrospinning/electrospray process/NA	NA	0.44	0.12	0.36	0.03	This study
		Coaxial electrospinning/NA		0.42	0.04	0.38	0.01	
TiO_2/PVDF	ITO/PET	Electrospinning/electrospray/ compression	NA	0.7	7.78	0.66	4.04	[17]
TiO_2/PP	FTO/glass	Extrusion-uniaxial stretching/NA	NA	0.12	0.0007	0.32	NA	[19] [38]
TiO_2	Ti foil	Anodization/Sintering	450	0.45	0.14	0.46	0.03	[39]
TiO_2	ITO/PET	Doctor blade	140	0.8	0.19	0.56	0.09	[41]

A significant challenge encountered during the fabrication of DSSC prototypes was the delamination of the electrospun layer from the ITO/PET substrate. Strong mechanical adhesion is critical to establish effective electrical contact between the semiconductor layer and the substrate, which is essential for high current generation [17] [42] [43]. Enhancing adhesion would not only improve flexibility but also prevent damage to the photoelectrode layer. This issue could be addressed through alternative pre-treatment or post-treatment techniques aimed at improving the adhesion of the mats, thereby enhancing the overall efficiency of the cells. For pre-treatment, atmospheric plasma treatment of polymeric substrates has been shown to significantly improve adhesion. Wante *et al.* [44] found that atmospheric plasma treatment of ITO/PEI substrates before depositing the TiO_2 layer significantly boosted the efficiency (η) of flexible DSSCs from 0.94%

(untreated) to 5.7% (treated). This improvement is attributed to enhanced adhesion, better charge transfer rates, and increased conductivity. For post-treatment, studies indicate that compression methods have strong potential to improve connectivity between semiconductor particles and electrical contact between the active layer and the substrate in flexible DSSCs [17] [45].

3.4. Electrochemical Impedance Spectroscopy (EIS) Characterization

An EIS study was carried out on DSSC prototypes to delve deeper into the electron recombination and electron transfer dynamics at the photoanode/dye/electrolyte interface. The Nyquist plots derived from the DSSCs, which were fabricated using flexible nanofibrous photoanode mats developed using CE and E-ES methods, along with their equivalent electrical circuits, are depicted in **Figure 6**. **Table 2** lists the series resistance (R_s) and charge-transfer resistance (R_{ct}) values determined from the fitting. In the electrochemical impedance spectrum, three distinct semicircular regions are typically observed: at low frequencies, the impedance characterizes the Warburg diffusion of the I_{3^-}/I_- redox couple within the electrolyte; at high frequencies, it reflects the charge transfer at the platinum counter electrode; and the semicircle at mid-frequencies indicates the charge transfer occurring at the interfaces between the photoanode, N719 dye, and electrolyte [46]. A larger semicircle diameter in this mid-frequency region suggests a higher charge transfer resistance (R_{ct}) [47]. In this study, the absence of the low-frequency semicircle can be attributed to the high porosity of the photoanode and the low viscosity of the electrolyte, which enhance ionic diffusion. This observation aligns with findings reported in the literature [48]. A comparison of the Nyquist plots indicates an enhancement in charge transfer at the photoanode/N719 dye/electrolyte interface for the DSSC prototype with the photoanode developed by the E-ES method. As shown in **Figure 6**, the corresponding Nyquist plot exhibits a smaller semicircle within the medium frequency range compared to that corresponding to the DSSC prototype with the photoanode developed via the CE method, signifying a reduction in charge transfer resistance. The smaller value of R_{ct} implies a faster electron transport with less charge accumulation at the photoanode/N719 dye/electrolyte interface [49]. This suggests that the positioning of TiO_2 nanoparticles on the fiber's surface contributes to a higher density of injected electrons with a lower recombination rate, leading to an increase in the short-circuit current density (J_{sc}) [50]. Additionally, R_1 or R_s in the equivalent circuit represents series resistance, identified as the origin of the first semicircle in the Nyquist plot. This component is linked to the sheet resistance of the conductive substrate, electrolyte resistance, and electrical contacts between TiO_2 nanoparticles and the conductive substrate [51] [52]. Both photoanodes developed by CE and E-ES methods exhibit high R_s values, aligning with findings in the literature for scenarios utilizing flexible ITO/PET substrates and low-temperature processes [41] [53]. Such outcomes are ascribed to the elevated sheet resistance of ITO/PET combined with the lack

of high sintering temperatures, which results in inadequate electrical contact between the composite's porous structure and the substrate. However, R_s value for E-ES process is higher than CE process. This result suggests that the reduced porosity in the case of E-ES, caused by the occlusion of micropores with TiO_2 agglomerates, hindered the movement of electrolyte ions, thereby increasing the ionic resistance of R_s. It is important to note that our results are consistent with findings in the literature, which indicate that the deposition technique significantly impacts R_s. Enhanced deposition techniques can improve surface morphology and charge transfer kinetics at the photoanode/dye/electrolyte interface, thereby lowering R_{ct}, while simultaneously increase R_s due to factors such as increased thickness, surface roughness, or non-uniform deposition of the TiO_2 layer [54] [55].

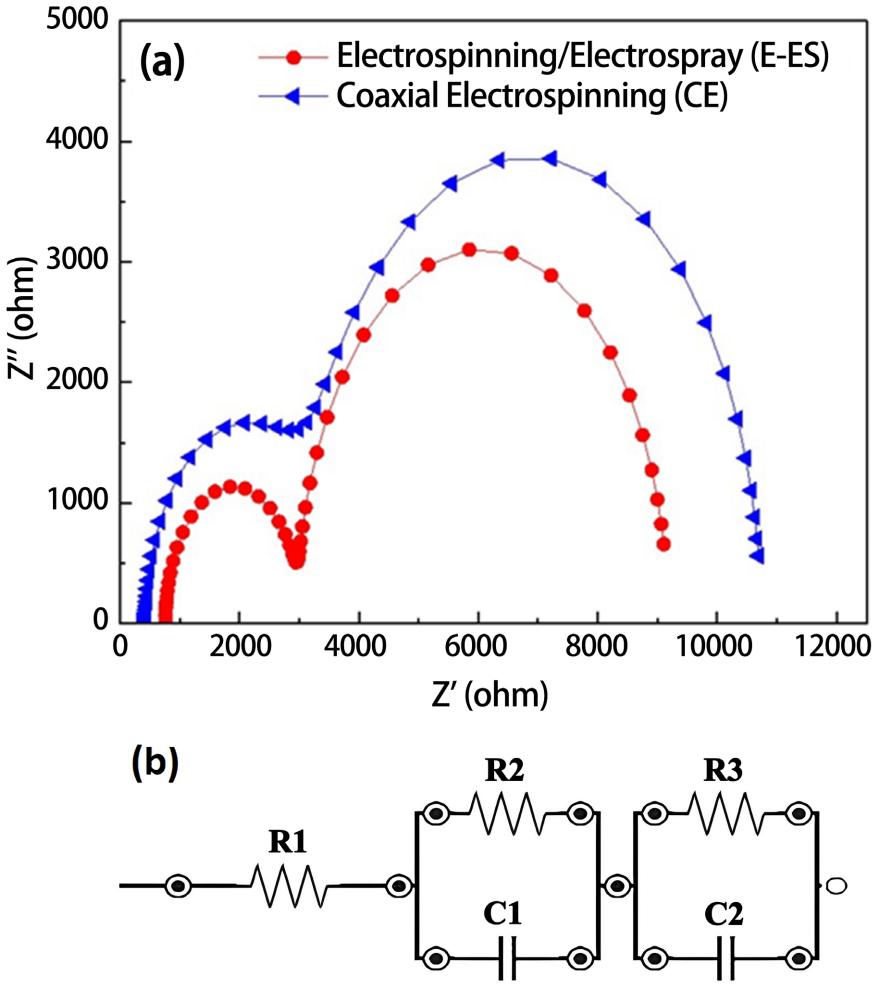

Figure 6. (a) Nyquist plots of DSSC prototypes prepared using flexible photoanodes developed via CE and E-ES methods; (b) Equivalent electrical circuit used for fitting the EIS spectra of the cells. This process was completed using ZView software. R_1 is series resistance, R_2 represents the electron-transfer resistance at the electrolyte/Pt counter electrode interface, and R_3 the electron transfer resistance at the photoanode/N719 dye/electrolyte interface.

4. Conclusion

A straightforward and cost-effective electrospinning method was employed to fabricate PET/TiO_2 nanocomposites at low temperatures, aiming to assess their efficacy as flexible fibrous photoanodes in Dye-Sensitized Solar Cells (DSSCs). TiO_2 nanobars were incorporated into the composite PET fibers through three electrospinning techniques (uniaxial electrospinning, coaxial electrospinning, and electrospinning-electrospraying), to meticulously manage their distribution within the composites. Our findings clearly demonstrate that, even though the mats developed by coelectrospinning (CE) show an improvement compared to those obtained via the method of uniaxial (UE) electrospinning, electrospinning-electrospraying (E-ES) method stands out for its potential to enhance composite quality and performance compared to the other two techniques explored. SEM images have provided clear evidence of a greater concentration of TiO_2 nanoparticles present on the surface of the PET nanofibers developed by E-ES method; a finding supported by EDX analysis. Consequently, the N719 dye adsorption capacity was improved by 110% and 337% in comparison to the PET/PET-TiO_2 core-shell nanofiber-based photoanode developed by both CE and UE methods, respectively. Furthermore, photovoltaic characterization has revealed that the short-circuit current density (J_{sc}) of DSSC prototypes with PET-TiO_2 photoanodes developed using the E-ES method saw a 200% increase over the coelectrospun PET/PET-TiO_2 core-shell nanofiberous photoanode developed using the CE method, leading to a substantial improvement in energy conversion efficiency. These findings underscore the critical role of TiO_2 nanoparticle positioning on the nanofiber surface in enhancing the performance of flexible PET/TiO_2 fibrous photoanodes. By making more TiO_2 nanoparticles accessible on the surface, N719 dye molecules have easier access, resulting in increased dye adsorption and, consequently, a higher J_{sc}.

Acknowledgements

The authors are grateful to the Natural Sciences and Engineering Research Council of Canada (NSERC), as well as the Research Center for High Performance Polymer and Composite Systems (CREPEC) for their financial support of this research. They also extend their thanks to Professor Bryan Koivisto from Toronto Metropolitan University for his assistance in DSSC prototype characterization.

Conflicts of Interest

The authors declare no conflicts of interest regarding the publication of this paper.

References

[1] Naik, P., Abdellah, I.M., Abdel-Shakour, M., Su, R., Keremane, K.S., El-Shafei, A., *et al.* (2018) Improvement in Performance of N3 Sensitized DSSCs with Structurally Simple Aniline Based Organic Co-Sensitizers. *Solar Energy*, **174**, 999-1007. https://doi.org/10.1016/j.solener.2018.09.071

[2] Aziz, N.A.S., Rahman, M.Y.A. and Umar, A.A. (2022) Comparative Study of Dye-Sensitized Solar Cell Utilizing Selenium and Palladium Cathode. *Journal of the Indian Chemical Society*, **99**, Article 100289. https://doi.org/10.1016/j.jics.2021.100289

[3] Zhang, P., Chu, F., Zhou, M., Tao, B. and Miao, F. (2024) DSSC Using Natural Dye Sensitized and Ag/CdS/TiO_2 Composite Structured Light Anode. *Vacuum*, **219**, Article 112763. https://doi.org/10.1016/j.vacuum.2023.112763

[4] Ye, M., Wen, X., Wang, M., Iocozzia, J., Zhang, N., Lin, C., *et al.* (2015) Recent Advances in Dye-Sensitized Solar Cells: From Photoanodes, Sensitizers and Electrolytes to Counter Electrodes. *Materials Today*, **18**, 155-162. https://doi.org/10.1016/j.mattod.2014.09.001

[5] Yang, H., Liu, W., Xu, C., Fan, D., Cao, Y. and Xue, W. (2019) Laser Sintering of TiO_2 Films for Flexible Dye-Sensitized Solar Cells. *Applied Sciences*, **9**, Article 823. https://doi.org/10.3390/app9050823

[6] Baiju, K.G., Murali, B., Subba Rao, R., Jayanarayanan, K. and Kumaresan, D. (2020) Heat Sink Assisted Elevated Temperature Sintering Process of TiO_2 on Polymer Substrates for Producing High Performance Flexible Dye-Sensitized Solar Cells. *Chemical Engineering and Processing-Process Intensification*, **149**, Article 107817. https://doi.org/10.1016/j.cep.2020.107817

[7] Sabet, M. and Jahangiri, H. (2017) Using a Low Temperature Method to Fabrication of Flexible Dye Sensitized Solar Cells with Three Different Counter Electrodes. *Journal of Materials Science: Materials in Electronics*, **29**, 778-783. https://doi.org/10.1007/s10854-017-7972-5

[8] Li, B., Huang, F., Zhong, J., Xie, J., Wen, M. and Peng, Y. (2016) Fabrication of Flexible Dye-Sensitized Solar Cell Modules Using Commercially Available Materials. *Energy Technology*, **4**, 536-542. https://doi.org/10.1002/ente.201500352

[9] Fan, R., Zhang, C., Yin, X., Xiong, Y., Xu, S., Yan, X., *et al.* (2017) Novel Flexible Photoanode Based on Ag Nanowire/Polymer Composite Electrode. *Journal of Materials Science*: *Materials in Electronics*, **28**, 10092-10097. https://doi.org/10.1007/s10854-017-6770-4

[10] Noorasid, N.S., Arith, F., Mustafa, A.N., Azam, M.A., Mahalingam, S., Chelvanathan, P., *et al.* (2022) Current Advancement of Flexible Dye Sensitized Solar Cell: A Review. *Optik*, **254**, Article 168089. https://doi.org/10.1016/j.ijleo.2021.168089

[11] Ahmad, M.S., Pandey, A.K., Rahim, N.A., Shahabuddin, S. and Tyagi, S.K. (2018) Chemical Sintering of TiO_2 Based Photoanode for Efficient Dye Sensitized Solar Cells Using Zn Nanoparticles. *Ceramics International*, **44**, 18444-18449. https://doi.org/10.1016/j.ceramint.2018.07.062

[12] Chen, L., Ke, C., Hon, M. and Ting, J. (2015) Electrophoretic Deposition of TiO_2 Coatings for Use in All-Plastic Flexible Dye-Sensitized Solar Cells. *Surface and Coatings Technology*, **284**, 51-56. https://doi.org/10.1016/j.surfcoat.2015.07.044

[13] Yamaguchi, T., Tobe, N., Matsumoto, D. and Arakawa, H. (2007) Highly Efficient Plastic Substrate Dye-Sensitized Solar Cells Using a Compression Method for Preparation of TiO_2 Photoelectrodes. *Chemical Communications*, No. 45, 4767-4769. https://doi.org/10.1039/b709911h

[14] Khir, H., Pandey, A.K., Saidur, R., Shakeel Ahmad, M., Abd Rahim, N., Dewika, M., *et al.* (2022) Recent Advancements and Challenges in Flexible Low Temperature Dye Sensitised Solar Cells. *Sustainable Energy Technologies and Assessments*, **53**, Article 102745. https://doi.org/10.1016/j.seta.2022.102745

[15] Sun, L., Chen, C., Hao, L., Wang, W., Zhao, Y. and Ye, Y. (2024) Antimony

Incorporated Flexible $Cu_2ZnSn(S,Se)_4$ Solar Cell for Enhanced Mechanical Endurance and Efficiency. *Vacuum*, **221**, Article 112902. https://doi.org/10.1016/j.vacuum.2023.112902

[16] Li, X., Zhao, Y. and Deng, C. (2010) Modification of TiO_2 Electrode Films in Dye-Sensitized Solar Cells with PMMA. *Journal of Sol-Gel Science and Technology*, **57**, 128-131. https://doi.org/10.1007/s10971-010-2332-4

[17] Li, Y., Lee, D., Kim, J.Y., Kim, B., Park, N., Kim, K., *et al.* (2012) Highly Durable and Flexible Dye-Sensitized Solar Cells Fabricated on Plastic Substrates: PVDF-Nanofiber-Reinforced TiO_2 Photoelectrodes. *Energy & Environmental Science*, **5**, 8950-8957. https://doi.org/10.1039/c2ee21674d

[18] Sa'adah, U., Himmah, S.W., Suprayogi, T., Diantoro, M., Sujito, S. and Nasikhudin, N. (2019) The Effect of Time Deposition of Pan/TiO_2 Electrospun on Photocurrent Performance of Dye-Sensitized Solar Cell. *Materials Today*: *Proceedings*, **13**, 175-180. https://doi.org/10.1016/j.matpr.2019.03.210

[19] Zohrevand, A., Ajji, A. and Mighri, F. (2014) Microstructure and Properties of Porous Nanocomposite Films: Effects of Composition and Process Parameters. *Polymer International*, **63**, 2052-2060. https://doi.org/10.1002/pi.4761

[20] Fang, J., Wang, X. and Li, T. (2011) Functional Applications of Electrospun Nanofibers. In: Lin, T., Ed., *Nanofibers-Production*, *Properties and Functional Applications*, IntechOpen Limited, 287-302. https://doi.org/10.5772/24998

[21] López-Covarrubias, J.G., Soto-Muñoz, L., Iglesias, A.L. and Villarreal-Gómez, L.J. (2019) Electrospun Nanofibers Applied to Dye Solar Sensitive Cells: A Review. *Materials*, **12**, Article 3190. https://doi.org/10.3390/ma12193190

[22] Mondal, K. (2017) Recent Advances in the Synthesis of Metal Oxide Nanofibers and Their Environmental Remediation Applications. *Inventions*, **2**, Article 9. https://doi.org/10.3390/inventions2020009

[23] Gallah, H., Mighri, F., Ajji, A. and Bandyopadhyay, J. (2023) Flexible PET/(PET-TiO_2) Core/Shell Nanofibrous Mats as Potential Photoanode Layer for Dye-Sensitized Solar Cells, DSSCs. *Materials Chemistry and Physics*, **305**, Article 127911. https://doi.org/10.1016/j.matchemphys.2023.127911

[24] Gallah, H., Mighri, F., Ajji, A. and Bandyopadhyay, J. (2020) Flexible Electrospun PET/TiO_2 Nanofibrous Structures: Morphology, Thermal and Mechanical Properties. *Polymers for Advanced Technologies*, **31**, 1612-1623. https://doi.org/10.1002/pat.4890

[25] Wali, Q., Bakr, Z.H., Manshor, N.A., Fakharuddin, A. and Jose, R. (2016) SnO_2-TiO_2 Hybrid Nanofibers for Efficient Dye-Sensitized Solar Cells. *Solar Energy*, **132**, 395-404. https://doi.org/10.1016/j.solener.2016.03.037

[26] Arifin, Z., Suyitno, S., Hadi, S. and Sutanto, B. (2018) Improved Performance of Dye-Sensitized Solar Cells with TiO_2 Nanoparticles/Zn-Doped TiO_2 Hollow Fiber Photoanodes. *Energies*, **11**, Article 2922. https://doi.org/10.3390/en11112922

[27] Virovska, D., Paneva, D., Manolova, N., Rashkov, I. and Karashanova, D. (2014) Electrospinning/Electrospraying vs. Electrospinning: A Comparative Study on the Design of Poly(L-Lactide)/Zinc Oxide Non-Woven Textile. *Applied Surface Science*, **311**, 842-850. https://doi.org/10.1016/j.apsusc.2014.05.192

[28] Lee, E., An, A.K., Hadi, P., Lee, S., Woo, Y.C. and Shon, H.K. (2017) Advanced Multi-nozzle Electrospun Functionalized Titanium Dioxide/Polyvinylidene Fluoride-Co-Hexafluoropropylene (TiO_2/PVDF-HFP) Composite Membranes for Direct Contact Membrane Distillation. *Journal of Membrane Science*, **524**, 712-720. https://doi.org/10.1016/j.memsci.2016.11.069

[29] Ahmad, S.H.A., Al-Ahmed, A., Hakeem, A.S., Alshahrani, T., Mahmood, Q.,

Mehmood, U., *et al.* (2021) Enhancing the Performance of Dye-Sensitized Solar Cell Using Nano-Sized Erbium Oxide on Titanium Oxide Photoanode by Impregnation Route. *Journal of Photochemistry and Photobiology*, **7**, Article 100047. https://doi.org/10.1016/j.jpap.2021.100047

[30] Charbonneau, C., Tanner, T., Davies, M.L., Watson, T.M. and Worsley, D.A. (2016) Effect of TiO_2 Photoanode Porosity on Dye Diffusion Kinetics and Performance of Standard Dye-Sensitized Solar Cells. *Journal of Nanomaterials*, **2016**, Article 9324858. https://doi.org/10.1155/2016/9324858

[31] Ani Melfa Roji, M., Ram Kumar, P., Sahaya Shajan, X. and Ajith Bosco Raj, T. (2023) Silver Doped $ZnSnO_3$/SnO Hybrid Nanostructures as DSSC Photoanodes: Charge Injection Dynamics, Slow Recombination Kinetics and Simulation Studies. *Optical Materials*, **138**, Article 113696. https://doi.org/10.1016/j.optmat.2023.113696

[32] Bhavani K.T., Joshi, D.N. and Dutta, V. (2021) Tandem DSSC Fabrication by Controlled Infiltration of Organic Dyes in Mesoporous Electrode Using Electric-Field Assisted Spray Technique. *Solar Energy*, **223**, 318-325. https://doi.org/10.1016/j.solener.2021.05.060

[33] Abrari, M., Ahmadi, M., Chenari, H.M. and Ghanaatshoar, M. (2024) Investigating the Effect of ZrO_2 Nanofibers in ZnO-Based Photoanodes to Increase Dye-Sensitized Solar Cells (DSSC) Efficiency: Inspecting the Porosity and Charge Transfer Properties in ZnO/ZrO_2 Nanocomposite Photoanode. *Optical Materials*, **147**, Article 114690. https://doi.org/10.1016/j.optmat.2023.114690

[34] Sufyan, M., Mehmood, U., Qayyum Gill, Y., Nazar, R. and Ul Haq Khan, A. (2021) Hydrothermally Synthesize Zinc Oxide (ZnO) Nanorods as an Effective Photoanode Material for Third-Generation Dye-Sensitized Solar Cells (DSSCs). *Materials Letters*, **297**, Article 130017. https://doi.org/10.1016/j.matlet.2021.130017

[35] Pourandarjani, A. and Nasirpouri, F. (2019) A New Approach to Understanding the Deficiency of Backside Illuminated Dye-Sensitized Solar Cells' Fill Factor as a Result of Cracking of the TNAs. *Materials Today: Proceedings*, **18**, 501-509. https://doi.org/10.1016/j.matpr.2019.06.238

[36] Li, Y., Yoo, K., Lee, D., Kim, J.H., Park, N., Kim, K., *et al.* (2010) Highly Bendable Composite Photoelectrode Prepared from TiO_2/Polymer Blend for Low Temperature Fabricated Dye-Sensitized Solar Cells. *Current Applied Physics*, **10**, e171-e175. https://doi.org/10.1016/j.cap.2010.01.014

[37] Zhang, P., Wu, C., Han, Y., Jin, T., Chi, B., Pu, J., *et al.* (2011) Low-Temperature Preparation of Hierarchical Structure TiO_2 for Flexible Dye-Sensitized Solar Cell. *Journal of the American Ceramic Society*, **95**, 1372-1377. https://doi.org/10.1111/j.1551-2916.2011.04984.x

[38] Zohrevand, A. (2014) Development of Polymer Nanocomposites Films and Their Potential for Photovoltaic Cell Applications, Ph.D. Thesis, Laval University.

[39] Hoseinzadeh, T., Solaymani, S., Kulesza, S., Achour, A., Ghorannevis, Z., Ţălu, Ş., *et al.* (2018) Microstructure, Fractal Geometry and Dye-Sensitized Solar Cells Performance of CdS/TiO_2 Nanostructures. *Journal of Electroanalytical Chemistry*, **830**, 80-87. https://doi.org/10.1016/j.jelechem.2018.10.037

[40] Duong Vu, T.T., Patel, J., Mighri, F., Do, T. and Ajji, A. (2015) The Effect of TiO_2 Surface Modification on the Photovoltaic Properties of Hybrid Bulk Heterojunction Solar Cells Based on MEH-PPV/CdS/TiO_2 Active Layer. *Green Processing and Synthesis*, **4**, 79-90. https://doi.org/10.1515/gps-2014-0092

[41] Longo, C., Nogueira, F., Cachet, H. and De Paoli, M. (2002) Solid-State and Flexible Solar Cells Based on Dye-Sensitized TiO_2: Study by Electrochemical Impedance

Spectroscopy. *Proceedings Volume* 4465, *Organic Photovoltaics II*, San Diego, 21 February 2002, 21-30. https://doi.org/10.1117/12.456936

[42] Sharif, N.F.M., Shafie, S., Ab. Kadir, M.Z.A., Hasan, W.Z.W., Mustafa, M.N. and Samaila, B. (2019) The Effect of Titanium (IV) Chloride Surface Treatment to Enhance Charge Transport and Performance of Dye-Sensitized Solar Cell. *Results in Physics*, **15**, Article 102725. https://doi.org/10.1016/j.rinp.2019.102725

[43] Rahman, M.M., Kang, H.C., Yoo, K. and Lee, J. (2022) Low-Temperature Chemical Sintered TiO_2 Photoanodes Based on a Binary Liquid Mixture for Flexible Dye-Sensitized Solar Cells. *Journal of Electrochemical Science and Technology*, **13**, 453-461. https://doi.org/10.33961/jecst.2022.00262

[44] Wante, H.P., Aidan, J. and Ling, Y.S. (2024) Highly Improved Efficiency of Flexible Dye Sensitized Solar Cells (DSSCs) by Non-Thermal Plasma Processing of PEI-ITO Polymer. *Optical Materials*, **150**, Article 115331. https://doi.org/10.1016/j.optmat.2024.115331

[45] Chen, H., Lin, C., Lai, Y., Chen, J., Wang, C., Hu, C., *et al.* (2011) Electrophoretic Deposition of ZnO Film and Its Compression for a Plastic Based Flexible Dye-Sensitized Solar Cell. *Journal of Power Sources*, **196**, 4859-4864. https://doi.org/10.1016/j.jpowsour.2011.01.057

[46] Qi, L., Wang, Q., Wang, T., Li, C., Ouyang, Q. and Chen, Y. (2012) Dye-Sensitized Solar Cells Based on ZnO Nanoneedle/TiO_2 Nanoparticle Composite Photoelectrodes with Controllable Weight Ratio. *Journal of Materials Research*, **27**, 2982-2987. https://doi.org/10.1557/jmr.2012.350

[47] Mehmood, U., Aslam, H.Z., Al-Sulaiman, F.A., Al-Ahmed, A., Ahmed, S., Malik, M.I., *et al.* (2016) Electrochemical Impedance Spectroscopy and Photovoltaic Analyses of Dye-Sensitized Solar Cells Based on Carbon/TiO_2 Composite Counter Electrode. *Journal of The Electrochemical Society*, **163**, H339-H342. https://doi.org/10.1149/2.0111606jes

[48] Wu, J., Lan, Z., Lin, J., Huang, M., Huang, Y., Fan, L., *et al.* (2017) Counter Electrodes in Dye-Sensitized Solar Cells. *Chemical Society Reviews*, **46**, 5975-6023. https://doi.org/10.1039/c6cs00752j

[49] Afzal, A.M., Bae, I., Aggarwal, Y., Park, J., Jeong, H., Choi, E.H., *et al.* (2021) Highly Efficient Self-Powered Perovskite Photodiode with an Electron-Blocking Hole-Transport NiO_x Layer. *Scientific Reports*, **11**, Article No. 169. https://doi.org/10.1038/s41598-020-80640-3

[50] Bhattacharjee, R. and Hung, I. (2014) Effect of Different Concentration Li-Doping on the Morphology, Defect and Photovoltaic Performance of Li-ZnO Nanofibers in the Dye-Sensitized Solar Cells. *Materials Chemistry and Physics*, **143**, 693-701. https://doi.org/10.1016/j.matchemphys.2013.09.055

[51] Oktaviani, E., Nursam, N.M., Shobih, Hidayat, J., Pranoto, L.M., Rosa, E.S., *et al.* (2021) Electrical and Electrochemical Properties of Sandwich- and Monolithic-Structured Dye-Sensitized Solar Cells with Various Counter Electrode Materials. *International Journal of Electrochemical Science*, **16**, Article 210922. https://doi.org/10.20964/2021.09.16

[52] Hoshikawa, T., Yamada, M., Kikuchi, R. and Eguchi, K. (2005) Impedance Analysis of Internal Resistance Affecting the Photoelectrochemical Performance of Dye-Sensitized Solar Cells. *Journal of The Electrochemical Society*, **152**, E68. https://doi.org/10.1149/1.1849776

[53] Castillo-Rodriguez, J., Ortiz, P.D., Mahmood, R., Gossage, R.A., Llanos, J., Espinoza, D., *et al.* (2023) The Development of Au-Titania Photoanode Composites toward

Semiflexible Dye-Sensitized Solar Cells. *Solar Energy*, **263**, Article 111955. https://doi.org/10.1016/j.solener.2023.111955

[54] Pan, M., Huang, N., Zhao, X., Fu, J. and Zhong, X. (2013) Enhanced Efficiency of Dye-Sensitized Solar Cell by High Surface Area Anatase-TiO_2-Modified P25 Paste. *Journal of Nanomaterials*, **2013**, Article 760685. https://doi.org/10.1155/2013/760685

[55] Özkacar, T., Taran, S., Gökçen, M. and Orhan, E. (2021) Annealing Effects of Photoanode on Dye Sensitized Solar Cell Performance. *Molecular Crystals and Liquid Crystals*, **724**, 102-110. https://doi.org/10.1080/15421406.2021.1910895